Proceedings of the Combustion Institute 42 (2026) 106089

Contents lists available at ScienceDirect

Proceedings of the Combustion Institute

journal homepage: www.elsevier.com/locate/proci

Suppression of intrinsic instabilities by strain in thermodiffusively unstable hydrogen flames

Alessandro Porcarelli [a,*], Pasquale E. Lapenna [b], Francesco Creta [b], Ivan Langella [a]

[a] Faculty of Aerospace Engineering, TU Delft, Kluyverweg 1, 2629HS, Delft, Netherlands
[b] Department of Mechanical and Aerospace Engineering, Sapienza, University of Rome, Via Eudossiana 18, 00189, Rome, Italy

ARTICLE INFO

Keywords:
Hydrogen premixed flames
Thermodiffusive instabilities
Strained flames
High-fidelity simulations
Weakly non-linear model

ABSTRACT

This study evaluates the effect of strain on the dynamic response of three-dimensional, thermodiffusively unstable lean premixed hydrogen flames. The analysis combines results obtained using a Sivashinsky-type weakly non-linear model in a stagnation-point flame configuration with fully non-linear, high-fidelity numerical simulations featuring detailed chemistry and transport in a counterflow reactants-to-products setup. The flame response to a polychromatic perturbation imposed along the third or 'extruded' dimension of the two strained configurations is evaluated in the linear regime. Results from both approaches reveal a stabilising effect with increasing strain, ultimately leading to the stabilisation of all the perturbation modes monitored at sufficiently high strain rate, which is linked to a strain-induced local flow redistribution in correspondence of positively and negatively curved flame fronts in the counterflow configuration. By integrating our previous findings in two-dimensional counterflow configurations (Porcarelli *et al*, Proc. Combust. Inst. 41 (2025) 105906) with the three-dimensional results presented here, we demonstrate for the first time that the onset of intrinsic flame instabilities in thermodiffusively unstable mixtures can be suppressed at sufficiently high strain rate conditions regardless of the direction of the imposed perturbation.

Novelty and significance statement

This study performs for the first time a linear stability analysis of three-dimensional, thermodiffusively unstable lean premixed hydrogen flames in strained configurations using both a weakly non-linear model and a fully non-linear model with detailed chemistry and transport. It is demonstrated that sufficiently high applied strain rate tends to suppress the onset of intrinsic instabilities in thermodiffusively unstable lean premixed hydrogen flames regardless of the direction of the imposed perturbation. This finding advances our understanding on the response to strain of lean premixed hydrogen flames, and suggests that strained configurations offer a viable strategy to control such flames in practical carbon-free and low-NO_x combustion systems.

1. Introduction

The global push towards hydrogen as a clean energy carrier has intensified research into the dynamics of lean premixed hydrogen flames, which are intrinsically unstable because of thermodiffusive effects [1]. This focus is driven by the need to control low-NO_x hydrogen flames in practical combustion systems.

Due to hydrogen's differential and preferential diffusion effects, lean premixed hydrogen flames are characterised by a distinctive response to strain [2,3] and curvature [4], which together define flame stretch. Unlike hydrocarbon fuels, sufficiently lean hydrogen/air mixtures have a Lewis number Le below the critical value Le_0 as defined by Bechtold and Matalon [5]. For these mixture conditions, the flame is characterised by a negative Markstein length, i.e. the flame speed increases with increased stretch. As a result, any imposed perturbation is amplified due to thermodiffusive effects, making the flame intrinsically unstable [6].

In the limit of small amplitude perturbations, an initial regime where the instability grows linearly in time can be identified, whose growth rate depends on the local perturbation mode, allowing to reconstruct the so-called 'dispersion relation'. The hydrodynamic theory allows the analytical derivation of the dispersion relation of intrinsically unstable flames [7,8]. However, this theory is incomplete for thermodiffusively unstable mixtures such as lean hydrogen/air. In the last decade, direct numerical simulations (DNS) based on comprehensive transport modelling have been thus performed to analyse both the

* Corresponding author.
E-mail address: a.porcarelli@tudelft.nl (A. Porcarelli).

https://doi.org/10.1016/j.proci.2026.106089
Received 13 March 2026; Accepted 5 June 2026
Available online 25 June 2026

linear and non-linear stability of thermodiffusively unstable lean hydrogen/air flames in a variety of flame setups, including two-dimensional [9–12] and three-dimensional [13,14] unstretched freely propagating flames, spherically expanding flames [15–17], and conical flames [18, 19]. The effects of stretch on the onset of intrinsic flame instabilities has been recently studied from the curvature point of view in spherically expanding flames, demonstrating the existence of a stabilising effect at small flame radii (high stretch) [17]. However, fewer studies exist addressing the flame dynamic response to tangential strain rate, i.e. the other contributor to stretch, and whether it induces a similar stabilisation effect remains thus unclear.

In a previous work [20], we performed a stability analysis of thermodiffusively unstable lean premixed hydrogen flames in a two-dimensional counterflow configuration, and found that any imposed perturbation is damped above a sufficiently high strain rate. In the present work, we extend this analysis to three-dimensional strained configurations 'extruded' in the third dimension with periodic boundary conditions. First, a preliminary assessment is performed over a stagnation point flame by means of a Sivashinsky-type weakly non-linear model [21]. Hence, the response of a lean premixed hydrogen flame to an imposed perturbation is evaluated in a three-dimensional counterflow configuration in the linear regime with a fully non-linear model, consisting of detailed-chemistry numerical simulations with comprehensive transport. Unlike [20], where the direction of the imposed perturbation was aligned with the flame-tangential velocity gradient established to strain the flame, here the perturbation is imposed in the third or 'extruded' dimension where the velocity component is an invariant. The purpose of this work is to determine whether sufficiently high strain suppresses the onset of intrinsic flame instabilities in thermodiffusively unstable mixtures regardless of the direction of the imposed velocity gradients established to strain the flame, thereby generalising our previous findings. This study focuses on laminar conditions to assess the potential for strained configurations to stabilise intrinsically unstable hydrogen flames, laying the groundwork for future investigations into their behaviour in practical turbulent combustion environments.

2. Computational models

2.1. Weakly non-linear model

G. Sivashinsky developed a family of weakly non-linear models which retain validity for thermodiffusively stable and unstable flames [21,22]. Sivashinsky et al. [23] later extended this model to account for the effect of strain in a stagnation point flame configuration. This model was derived under the assumption of constant density flow and thus neglects thermal expansion across the flame. Despite this strong assumption, this model is retained here as it provides useful information on the linear stability characteristics of thermodiffusively unstable flames in three-dimensional stagnation point configuration, and on how their dynamic response is affected by increasing strain rate.

Fig. 1 illustrates the stagnation point configuration considered for the analysis in the present work. The prescribed velocity field implies a uniform strain rate K_s on the flame. The flame front, nominally planar and oriented perpendicularly to the x axis, is located at a fixed distance from the stagnation surface and is stretched along the y direction. The flow in the present configuration is homogeneous in the third dimension, z. Small corrugations of the flame front are described by the leading-order perturbation $\psi(\eta, \zeta, \tau)$, where η and ζ are rescaled coordinates along the flame surface in the y and z directions, respectively, and τ is a rescaled time coordinate. Perturbations are thus modelled as:

$$(\psi)_\tau + 4\nabla^4(\psi) + \nabla^2(\psi) + \frac{1}{2}(\nabla\psi)^2 + \alpha(\eta\psi)_\eta = 0, \tag{1}$$

where the subscripts in the first and last term refer to derivatives with respect to τ and η, respectively. The equation above can be integrated

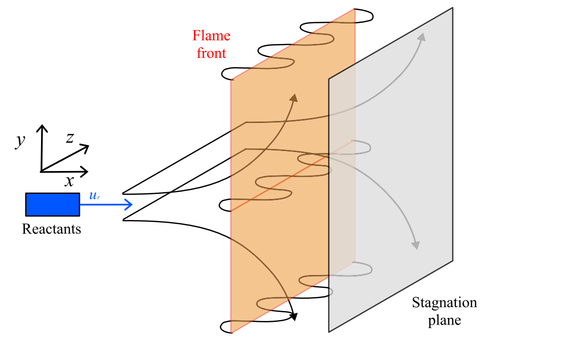

Fig. 1. Sketch of the three-dimensional stagnation-point flame setup simulated with the weakly non-linear model with imposed perturbation along the z direction.

via a pseudo-spectral approach as described in [24]. The biharmonic term $4\nabla^4(\psi)$ is stabilising and accounts for short-wavelength diffusive effects. The Laplacian term $\nabla^2(\psi)$ is destabilising and represents the effect of thermodiffusive instability driven by differential diffusion of heat and reactant. Note that the hydrodynamic instability is not taken into account as the model assumes constant density. The non-linear term $\frac{1}{2}(\nabla\psi)^2$ describes the effect of self-advection of the flame front and continuously regenerates short-wavelength perturbations through mode interaction, making the problem non-linear. The last term $\alpha(\eta\psi)_\eta$ represents flame stretch due to the stagnation-point flow. The equation is derived through a matched asymptotic expansion in powers of ε near the thermodiffusive instability threshold $Le \sim 1$, where $\varepsilon = 0.5$ is a consistent thermodifussive instability parameter as discussed in [25]. Strain rate enters the evolution equation at the same order as the thermodiffusive instability through the scaled parameter $\alpha = K_s/\varepsilon^2$. Different strain rates can thus be prescribed through the parameter α from unstrained conditions ($\alpha = 0$) to $\alpha = 65$ in the present study. Imposing a similar polychromatic methodology to that used for high-fidelity simulations (see Section 2.2) across the z direction, the dispersion relation is reconstructed in the linear regime by tracking in time an appropriately scaled non-dimensional growth rate ω of each of the $N = 128$ perturbation modes identified by the non-dimensional wavenumber k.

2.2. Fully non-linear model

High-fidelity, laminar reacting flow simulations are performed with detailed chemistry using an in house low-Mach version of reactingFoam. In Einstein's notation, the equation solved for the generic species k reads

$$\frac{\partial(\rho Y_k)}{\partial t} + \frac{\partial(\rho u_i Y_k)}{\partial x_i} = -\frac{\partial(\rho V_{k,i} Y_k)}{\partial x_i} + W_k \dot{\omega}_k, \tag{2}$$

where ρ is the mixture density, $V_{k,i}$ is the diffusion velocity of species k, $\dot{\omega}_k$ is the molar rate of production of species k, W_k is the molar mass of species k, and subscript i denotes the spatial directions. Our implementation introduced a mixture-averaged diffusion model with velocity correction and temperature-dependent species thermodynamic and transport properties as detailed and validated in [20]. Soret effect is neglected to reduce computational cost coherently to our previous work [20], where we found that this assumption has a negligible impact on the quantitative predictions of the perturbation growth rates in the linear regime (see Section 2.1 in [20]). Detailed kinetic data of reactions and species transport are taken from the Conaire chemical mechanism [26].

The setup consists of a lean premixed hydrogen/air flame (equivalence ratio $\phi = 0.5$) in a two-dimensional counterflow reactants-to-products configuration as the one described in Porcarelli et al. [20],

Table 1
Overview of the simulations investigated in the present work.

Case name	a [s^{-1}]	s_c [m/s]	δ_f [mm]	τ_f [ms]	Ka [–]
Unstrained	0	0.485	0.405	0.834	0
a2000	1447.5	0.732	0.346	0.472	1.2078
a5000	3633.5	0.831	0.299	0.360	3.0570

which is 'extruded' in the third dimension by $L_z = 2$ cm $\simeq 49\delta_{f,u}$, where $\delta_{f,u}$ is the unstretched laminar flame thickness. A sketch is provided in Fig. 2. Periodic boundary conditions are prescribed along the z direction. Note that to reduce the computational cost, we reduced the domain dimension in the y direction from 2 cm as done in [20] to 1 cm in this study, as we will not impose any perturbation along this direction. Note that the results of the stability analysis in the linear regime are unaffected by the domain size [12]. The third dimension is discretised with a uniform mesh of 800 finite volumes, such that a uniform mesh of 800 × 400 × 800 elements with $\Delta x = 2.5 \cdot 10^{-5}$ m is achieved in all directions. The nominal applied strain rate in this configuration is defined as

$$a = \frac{|u_r| + |u_p|}{L_x}, \tag{3}$$

where $L_x = 2$ cm is the domain length in the x direction, and u_r and u_p are the velocities at the reactants and products boundary, respectively. Two levels of strain $a = 1447.5$ s^{-1} and $a = 3633.5$ s^{-1} are considered in this study, matching the two highest strain rate cases in [20]. Note that these strain rate values are not directly comparable to the those chosen for α in the weakly non-linear model, which is a scaled parameter (see Section 2.1). A summary of the cases investigated along with their consumption speed s_c, thermal flame thickness δ_f, chemical time scale τ_f, and Karlovitz number is provided in lines 2 and 3 of Table 1. The Karlovitz number is defined as $Ka = a\delta_{f,u}/s_L$, where s_L is the laminar flame speed (corresponding to the unstretched consumption speed $s_{c,u}$). Note that the values in the case names refer to the flamelet strain rate according to the definition in a one-dimensional counterflow flamelet equation framework [2], as explained in Section 1 of the Supplementary Material, which also reports strain rate values obtained using other definitions from literature. The computations are performed with a third-order cubic scheme for the convective term of all resolved quantities, combined with an implicit second-order Crank–Nicolson discretisation scheme for time marching. A constant time-step is chosen to ensure a maximum CFL number below 0.2. Unlike in freely-propagating unstrained setups, here the basic state solution is obtained from two-dimensional counterflow simulations at $a = 1447.5$ s^{-1} and $a = 3633.5$ s^{-1} in [20] after they achieved a steady state with a stabilised flat flame, and is mapped over the 3D domain as starting solution for the 3D simulations. Then, the flame is perturbed across the z direction with a multi-wavelength perturbation of $N = 42$ modes with initial amplitude $A_0 = 0.02\delta_f$, and the dispersion relation in the linear regime is reconstructed following the polychromatic methodology by Al Kassar et al. [12]. Note that the strain rates selected for this work exceed the threshold set in [20] ($a \gtrsim 700$ s^{-1}) required to obtain a steady, stabilised flat flame in 2D, enabling its use as initial solution for perturbation after mapping in 3D. For comparison, the results of an unstrained 2D freely propagating flame obtained in [20, Sec. 3.1] are also evaluated. A summary of the flame parameters for this case, which will be indicated with the subscript u in the remainder of this work, are reported in Table 1. It is worth noting that there is no coupling between multi-dimensional perturbations in the linear regime, thus the linear stability analysis for this 2D setup is still relevant for comparison to that performed for the 3D cases presented in this work [27].

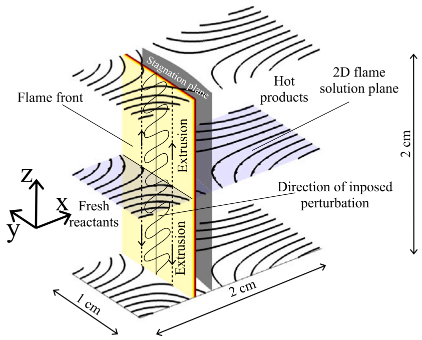

Fig. 2. Sketch of the three-dimensional counterflow setup simulated with the fully non-linear model with imposed perturbation along the z direction. The flame front is identified by the thick surface coloured with the yellow-to-red colourmap, representing the reactive region of the domain.

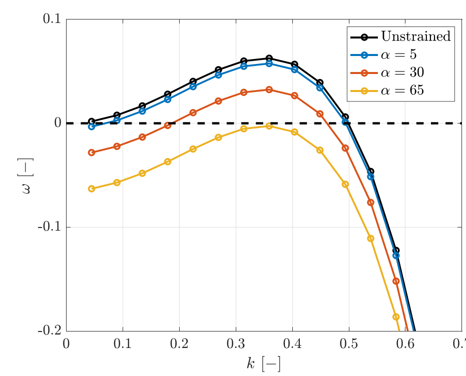

Fig. 3. Dispersion relation for perturbations imposed along the z direction of unstrained and different strained three-dimensional stagnation point flames, obtained with the weakly non-linear model described in Section 2.1.

3. Results and discussion

3.1. Weakly non-linear model

The dispersion relation obtained numerically with the extended weakly non-linear model from Sivashinsky et al. [23] are reported for different strain rates in Fig. 3 for the three-dimensional stagnation point flame configuration described in Section 2.1. Note that the reported results refer to the growth rate of the different modes for an imposed perturbations along the z direction, which is perpendicular to the flame-tangential velocity gradient established to strain the flame (y direction). Also note that since thermal expansion is neglected in the model (see Section 2.1), the curves exhibit a zero derivative in the limit of zero wavenumber ($\partial\omega/\partial k|_{k=0} = 0$).

The figure shows that the growth rate of each mode is diminished with increasing strain rate. This indicates that the modes which are intrinsically unstable in unstrained conditions progressively become stable under the effect of strain. Ultimately, at the highest strain rate conditions investigated ($\alpha = 65$), all modes feature a stabilising negative growth rate. These results suggest that sufficiently high strain rate can suppress the onset of intrinsic instabilities growing in the direction perpendicular to that of the flame-tangential velocity gradients established to strain the flame. These findings provide a first qualitative assessment of the effect of strain in thermodiffusively unstable flames. However, it is worth noting that the weakly non-linear model has been shown to hold only under conditions of weak stretch [28] and near-unity Lewis number [29]. Additionally, the stagnation point configuration may lose reliability at high strain rates due to the flame being pushed towards the wall, potentially leading to unpredictable flame-wall interactions [20].

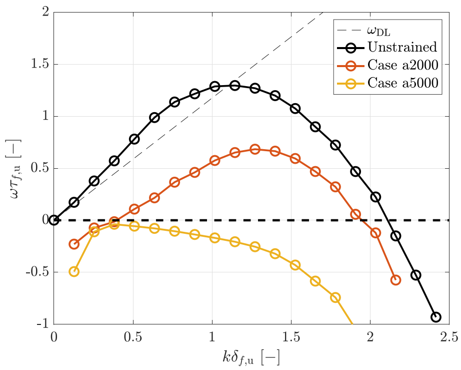

Fig. 4. Dispersion relation obtained over an iso-line at $c = c(\dot{\omega}_c^{max})$ in the plane $y = 0$ for unstrained and different strained three-dimensional counterflow lean premixed hydrogen flames. The axes are scaled with the unstretched laminar flame thickness $\delta_{f,u}$ and chemical time scale $\tau_{f,u}$ (see Table 1).

To draw robust conclusions, high-fidelity numerical simulations based on a fully non-linear model with detailed chemistry and transport are therefore required, as discussed in the following subsection.

3.2. Fully non-linear model

The results obtained with the 3D simulations described in Section 2.2 are presented here. Unlike in our previous work [20], where the perturbation was imposed along the same direction as the flame-tangential velocity gradient established to strain the flame (y direction), the perturbation is now applied perpendicular to that gradient (along the z direction). Since the 'extruded' counterflow configuration features a zero velocity component in the z direction ($u_z = 0$), any perturbation applied to the flame along this direction will not be affected by the velocity field. This means that the flame will not feature any mode shift, which is the case for perturbations along the y direction. This allows to perform a classical linear stability analysis and reconstruct a dispersion relation as in a freely propagating flame. The growth rate ω of a perturbation mode identified by the wavenumber k is defined as

$$\omega = \frac{1}{A}\frac{dA}{dt}, \tag{4}$$

where A is the amplitude of a given k evolving in time t. The amplitude data are sampled in time over an iso-line in the plane $y = 0$ identified by the iso-line of progress variable c where the corresponding reaction rate $\dot{\omega}_c$ is maximum in unperturbed conditions. Here, the progress variable is defined based on the water mass fraction:

$$c = \frac{Y_{H_2O}}{Y_{H_2O}^{max}}. \tag{5}$$

Note that due to the computational time to let flame fingers develop in the non-linear growth regime, the analysis in this study is limited to the linear growth regime.

The dispersion relations for the unstrained and strained cases of Table 1 are reported in Fig. 4, together with the growth rate of hydrodynamic or Darrieus–Landau instabilities $\omega_{DL} = ((\sigma^3+\sigma^2-\sigma)^{1/2}-\sigma)/(1+\sigma)$ as defined in [8], where $\sigma = \rho_0/\rho_b$ is the thermal expansion coefficient.

The graph shows that the dispersion relation curve is shifted downwards with increasing strain, validating the trend obtained with the weakly non-linear model in Section 3.1. This indicates that for a given perturbation mode, the associated growth rate decreases. Furthermore, in the lower strain rate case, some of the lower wavenumber and higher wavenumber modes that are unstable in unstrained conditions become stable, displaying negative growth rates. More interestingly, for the highest strain rate case all the modes become stable, confirming the finding obtained preliminarily with the weakly non-linear model. The reader can find the time evolution of modal amplitude $A(k)$ for cases a2000 and a5000 in Section 2 of the Supplementary Material.

To understand how the observed shift of the dispersion relation curve with increasing strain affects the global flame wrinkling, the probability density function (PDF) of the local curvature sampled across the same iso-line is reported in Fig. 5. The PDF is evaluated both at the beginning ($t = 2.4\tau_{f,u}$, Fig. 5(a)) and towards the end of the linear regime ($t = 3.6\tau_{f,u}$, Fig. 5(b)), and is normalised such that $\int_{k_{min}}^{k_{max}} P_k d\kappa = 1$ to allow the comparison between the two instants. These two instants are identified by inspecting the time ranges of constant growth rate for each mode in the three cases (not shown). The graphs show that for the highest strain case and at the beginning of the linear regime, the range of curvature values with significant probability is substantially narrower, suggesting that the flame front is characterised by less pronounced local curvature values compared to the unstrained and lower strain cases. At the later instant towards the end of the linear regime, the range of curvature values with significant probability is wider compared to the previous instant for the unstrained and a2000 cases, indicating that the local curvature has increased in time due to the growth of intrinsic flame instabilities. In the moderate strain case a2000, however, the widening is less pronounced as expected from its dispersion relation (see Fig. 4), which exhibits lower growth rates and a restricted range of unstable modes compared to the unstrained case. Yet, most of the modes are still unstable, which explains why the curvature range still widens in time. In contrast, the range of curvature values with significant probability has further narrowed at the later instant for case a5000, indicating that the curvature is decreasing everywhere across the flame front and thus that the flame is restoring its initial flat shape. Visual evidence of increasing and decreasing local curvature in time is further provided for cases a2000 and a5000, respectively, in Section 3 of the supplementary material. Combined with the observed shift in the dispersion relation towards negative growth rates at all modes (see Fig. 4), these findings demonstrate that sufficiently high strain rate is able to suppress the onset of intrinsic instabilities along the direction perpendicular to the flame-tangential velocity gradient established to strain the flame, thereby confirming the behaviour suggested by the weakly non-linear model. The mechanism underlying this suppression is explored in the following sections.

3.3. Reaction rate distribution

Flame contours for cases a2000 and a5000 of Table 1 are shown in Fig. 6 at an instant at the beginning of the linear regime ($t = 2.4\tau_{f,u}$). The flame is identified here as the iso-surface at the value of progress variable where its reaction rate would peak in unperturbed conditions. The surface is coloured with the progress variable reaction rate $\dot{\omega}_c$ to identify the regions of higher and lower reactivity. The lower strain rate case exhibits the typical reaction rate pattern of an intrinsically unstable flame front due to the thermodiffusive mechanism. Indeed, positively (negatively) curved flame regions, i.e. concave towards the products (reactants), are characterised by increased (decreased) reaction rates, which enable the onset of the instabilities. Since instabilities are suppressed for the higher strain case (see Section 3.2), one might expect that an opposite behaviour occurs in this case. However, Fig. 6(b) shows that the reaction rate still increases (decreases) in positively (negatively) curved flame regions, albeit its variation is less pronounced due to the more limited curvature range. This finding suggests that the observed suppression phenomenon is not due to thermodiffusive mechanisms being reversed by macroscopic strain, but is rather linked to possible strain-induced modifications of the local flow field where the curved flame regions are located, which can result in a stabilising hydrodynamic effect competing with the onset of intrinsic instabilities. This aspect is investigated next.

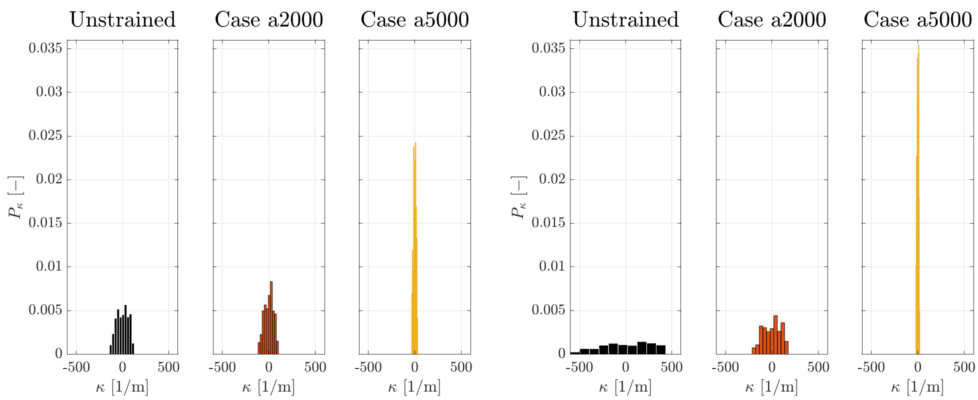

(a) $t = 2.4\tau_{f,u}$.

(b) $t = 3.6\tau_{f,u}$.

Fig. 5. Normalised PDF of curvature P_κ over an iso-line at $c = c(\dot{\omega}_c^{\max})$ in the plane $y = 0$ for the three different strain rate cases in Table 1. The PDF is evaluated at two different timesteps: (a) at the beginning of the linear regime, and (b) towards the end of the linear regime.

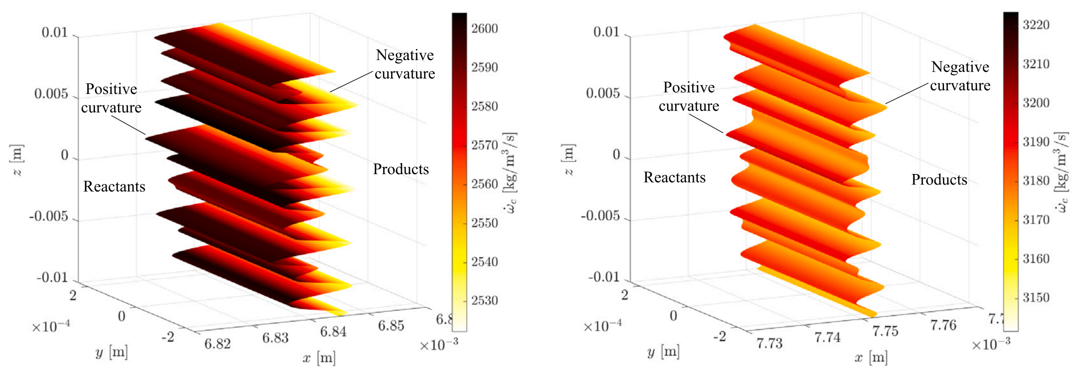

(a) Case a2000.

(b) Case a5000.

Fig. 6. Flame surface (iso-surface at $c_{H_2O} = c(\dot{\omega}_{c,\max})$) for cases a2000 (a) and a5000 (b) in Table 1 in a subdomain in the y direction coloured with the progress variable reaction rate $\dot{\omega}_c$.

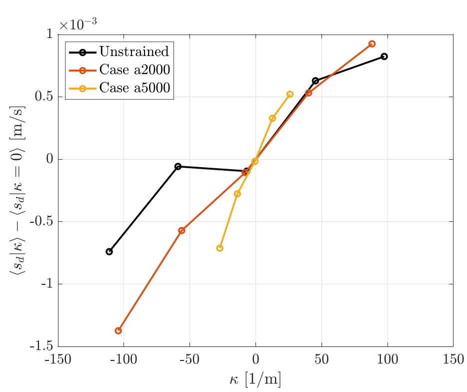

Fig. 7. Conditional mean of the density-scaled displacement speed s_d on curvature κ for the three different strain rate cases in Table 1. The conditional mean is evaluated at an instant at the beginning of the linear regime ($t = 2.4\tau_{f,u}$) over an iso-line at $c_{H_2O} = c(\dot{\omega}_{c,\max})$ in the plane $y = 0$.

3.4. Displacement speed analysis

An investigation on the correlation between the local displacement speed and curvature across the flame front is performed in this section. The displacement speed measures the flame front speed relative the flow and is defined as

$$s_d = \frac{\rho}{\rho_0}\left[\frac{1}{|\nabla c|}\frac{Dc}{Dt}\right] = \frac{\rho}{\rho_0}\left[\frac{1}{|\nabla c|}\left(\frac{\partial c}{\partial t} + \mathbf{u}\cdot\nabla c\right)\right], \tag{6}$$

where ρ_0, ρ, and $\mathbf{u}$ are the density of the unburnt mixture, the local density, and the local velocity vector, respectively [30]. Note that the expression above is scaled with the density ratio ρ/ρ_0 to account for thermal expansion across flame front. The local curvature of the flame front is defined as

$$\kappa = \nabla\cdot\mathbf{n}, \tag{7}$$

where $\mathbf{n} = -\nabla c/|\nabla c|$ is the unit vector normal to the flame front, which is positive when pointing towards the reactants. The conditional mean of the displacement speed on curvature $\langle s_d|\kappa\rangle$ for the three cases of Table 1 is reported in Fig. 7. The sample points to compute the conditional mean are taken on the same iso-line identified in Section 3.2 at an instant at the beginning of the linear regime for the three cases ($t = 2.4\tau_{f,u}$). For an evaluation of the displacement speed trends at a later instant ($t = 3.6\tau_{f,u}$), the reader is referred to Section 4 of the Supplementary Material. To compare the curves at different strain rates, the value at zero curvature $\langle s_d|\kappa = 0\rangle$ is subtracted to the conditional mean values. The figure shows that the dependence of the displacement speed on the local curvature remains mainly unaffected as the strain rate varies. In an intrinsically unstable case, the positively (negatively) curved flame fronts are expected to locally propagate at increased (decreased) flame speeds, enabling the onset of the instability. The positive correlation observed between displacement speed and curvature in the unstrained and a2000 cases confirms this expectation. Conversely, positively (negatively) curved flame fronts maintain an increased (decreased) flame speed for the case a5000 of Table 1, i.e. this case has the characteristics of an intrinsically unstable flame despite the analysis in Section 3.2 showed that it is stable.

In order further shed light on this point, it is convenient to decompose the density-scaled displacement speed into two different velocity components as follows [30]:

$$s_d = s_a + u_{\mathrm{n}} = s_a + \frac{\rho}{\rho_0}(-\mathbf{u}\cdot\mathbf{n}) = \frac{\rho}{\rho_0}\left(\frac{1}{|\nabla c|}\frac{\partial c}{\partial t} + \mathbf{u}\cdot\frac{\nabla c}{|\nabla c|}\right). \tag{8}$$

The first term s_a in Eq. (8) represents the absolute speed of the flame front, corresponding to its velocity relative to the laboratory frame. The second term $u_{\mathrm{n}} = \rho/\rho_0(-\mathbf{u}\cdot\mathbf{n})$ is the density weighted local flow velocity encountered by the flame front along its normal direction. The conditional mean of these two components are reported in Fig. 8 at the iso-line sampling points. Both the components exhibit an opposite behaviour with increasing curvature for the a5000 case which is intrinsically stable as compared to the other unstable cases. In a case with growing instabilities, i.e. with increasing perturbation amplitude in time, a positively (negatively) curved flame front is expected to propagate upstream (downstream) in the domain towards the reactants (products) with respect to the laboratory frame, which means it should exhibit an increased (decreased) absolute speed (recall that $\mathbf{n} > 0$ when pointing towards the reactants). This behaviour is indeed observed in the unstrained and a2000 cases. On the contrary, in an intrinsically stable case, a positively (negatively) curved flame front should feature a decreased (increased) absolute speed to enable the amplitude of the instabilities to decrease in time with respect to the laboratory frame, which is the behaviour observed for case a5000. Note that since the absolute speed is measured with respect to the laboratory framework, its variations as a function of curvature are orders of magnitude smaller than the laminar flame speed or the consumption speed, which are instead quantified with respect to the flow field. Yet, these variations are meaningful to identify unequivocally whether the instability at a positively/negatively curved flame front is growing or damping. Let us now consider the local flow velocity component normal to the flame front locally (right plot in Fig. 8). For the two unstable cases, the graph shows that a positively (negatively) curved flame region encounters a decreased (increased) local flow velocity normal to the flame front. This flow distribution with local curvature allows the instability to grow from an hydrodynamic perspective, as the local flow field does not 'oppose' to the positively (negatively) curved flame front upstream (downstream) propagation. Notably, the a2000 case exhibits a significantly weaker negative correlation compared to the unstrained case, suggesting that strain is playing a role in altering the local flow field encountered by the flame front. This trend is instead inverted for the higher strain case a5000. Here, positively (negatively) curved flame fronts encounter regions of locally increased (decreased) normal flow velocity which counteracts their upstream (downstream) propagation, thereby preventing the instabilities to grow and instead enabling a suppression mechanism. This analysis suggests that the observed suppression of intrinsic instabilities by strain might be linked to a configuration-based local flow redistribution in correspondence of positively/negatively curved flame fronts, which enables a stabilising hydrodynamic effect competing with Darrieus–Landau and thermodiffusive mechanisms, rather than to local thermodiffusive effects being suppressed by strain.

4. Conclusions

This study revealed through complementary modelling approaches a stabilising effect of strain on perturbations imposed along the perpendicular direction to the flame-tangential velocity gradient in three-dimensional strained flame configurations. The analysis of the correlation between the local reaction rate and displacement speed with curvature along the flame front revealed that the stabilisation mechanism is not due to thermodiffusive effects being mitigated, but is rather linked to hydrodynamic effects enabled by a strain-induced local flow redistribution in correspondence of positively and negatively curved flame fronts in the counterflow configuration.

These results enable the generalisation of the findings of our previous work, where we observed that any perturbation imposed along the direction of the velocity gradient is damped at sufficiently high strain rate in two-dimensional counterflow configurations. It can be concluded that the onset of intrinsic flame instabilities in thermodiffusively unstable mixtures can be suppressed by sufficiently high strain rate regardless of whether the imposed perturbation is aligned or misaligned with the flame-tangential velocity gradient established to strain the flame. Ultimately, it is demonstrated for the first time with high-fidelity numerical simulations that sufficiently high strain rate can stabilise lean premixed hydrogen flames that would be otherwise intrinsically unstable. This finding paves the way for leveraging strained configurations as a stabilisation strategy, enabling effective control of intrinsic flame instabilities in practical turbulent lean premixed hydrogen combustion systems. In this framework, future works should focus on investigating whether the strain-induced instability suppression mechanism observed in this study is linked to a suppression of synergistic effects in turbulent settings.

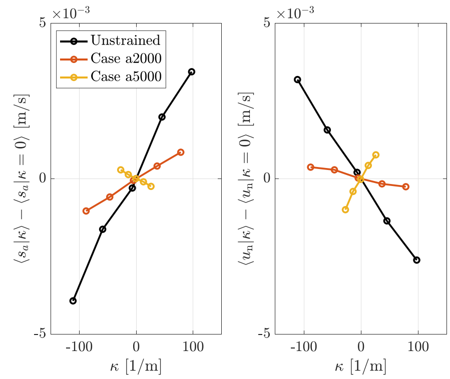

Fig. 8. Conditional mean of the absolute speed (s_a) and local flow velocity (u_{n}) components of the displacement speed versus curvature for the three different strain rate cases in Table 1. The conditional mean is evaluated at an instant at the beginning of the linear regime ($t = 2.4\tau_{f,u}$) over an iso-line at $c = c(\dot{\omega}_c^{\max})$ in the plane $y = 0$.

CRediT authorship contribution statement

Pasquale E. Lapenna: Writing – review & editing, Supervision, Methodology, Formal analysis, Conceptualization. **Francesco Creta:** Writing – review & editing, Supervision, Methodology, Formal analysis, Conceptualization. **Ivan Langella:** Writing – review & editing, Supervision, Project administration, Funding acquisition, Conceptualization. **Alessandro Porcarelli:** Conceptualisation, Software, Formal analysis, Investigation, Data curation, Writing – original draft.

Declaration of competing interest

The authors declare that they have no known competing financial interests or personal relationships that could have appeared to influence the work reported in this paper.

Acknowledgements

AP and IL gratefully acknowledge financial support from the ERC Starting Grant OTHERWISE, grant n. 101078821, and the Dutch Ministry of Education and Science for providing funding support via the

Sector Plan scheme. AP further acknowledges financial support to perform Short Term Scientific Mission (STSM) at Sapienza (Rome) from the CYPHER consortium (COST ACTION CA22151). PEL and FC acknowledge financial support by ICSC (Centro Nazionale di Ricerca in HPC, Big Data and Quantum Computing) funded by the European Union – NextGenerationEU. The authors also acknowledge the use of the Dutch National Supercomputer Snellius grant NWO-2023.044 to perform the simulations.

Appendix A. Supplementary data

Supplementary material related to this article can be found online at https://doi.org/10.1016/j.proci.2026.106089.

References

[1] H. Pitsch, The transition to sustainable combustion: Hydrogen-and carbon-based future fuels and methods for dealing with their challenges, Proc. Combust. Inst. 40 (1–4) (2024) 105638.
[2] A. Porcarelli, I. Langella, Mitigation of preferential diffusion effects by intensive strain in lean premixed hydrogen flamelets, Proc. Combust. Inst. 40 (1–4) (2024) 105728.
[3] M.R. Acquaviva, A. Porcarelli, I. Langella, Influence of soret effect on flame structure and NOx emissions in highly strained lean premixed counterflow hydrogen flames, Fuel 395 (2025) 134939.
[4] E. Varea, J. Beeckmann, H. Pitsch, Z. Chen, B. Renou, Determination of burning velocities from spherically expanding H2/air flames, Proc. Combust. Inst. 35 (1) (2015) 711–719.
[5] J. Bechtold, M. Matalon, The dependence of the Markstein length on stoichiometry, Combust. Flame 127 (1–2) (2001) 1906–1913.
[6] P.E. Lapenna, L. Berger, F. Creta, H. Pitsch, Hydrogen laminar flames, in: Hydrogen for Future Thermal Engines, Springer, 2023, pp. 93–139.
[7] M. Matalon, B.J. Matkowsky, Flames as gasdynamic discontinuities, J. Fluid Mech. 124 (1982) 239–259.
[8] M. Matalon, C. Cui, J. Bechtold, Hydrodynamic theory of premixed flames: Effects of stoichiometry, variable transport coefficients and arbitrary reaction orders, J. Fluid Mech. 487 (2003) 179–210.
[9] C.E. Frouzakis, N. Fogla, A.G. Tomboulides, C. Altantzis, M. Matalon, Numerical study of unstable hydrogen/air flames: Shape and propagation speed, Proc. Combust. Inst. 35 (1) (2015) 1087–1095.
[10] L. Berger, A. Attili, H. Pitsch, Intrinsic instabilities in premixed hydrogen flames: Parametric variation of pressure, equivalence ratio, and temperature. Part 1-dispersion relations in the linear regime, Combust. Flame 240 (2022) 111935.
[11] L. Berger, A. Attili, H. Pitsch, Intrinsic instabilities in premixed hydrogen flames: Parametric variation of pressure, equivalence ratio, and temperature. Part 2–Non-linear regime and flame speed enhancement, Combust. Flame 240 (2022) 111936.
[12] S. Al Kassar, L. Berger, P.E. Lapenna, F. Creta, H. Pitsch, A. Attili, Efficient and accurate calculation of dispersion relations for intrinsically unstable premixed flames, Combust. Flame 269 (2024) 113640.
[13] X. Wen, L. Berger, L. Cai, A. Parente, H. Pitsch, Thermodiffusively unstable laminar hydrogen flame in a sufficiently large 3D computational domain–Part I: Characteristic patterns, Combust. Flame 263 (2024) 113278.
[14] T. Zirwes, F. Zhang, T.L. Kaiser, K. Oberleithner, O.T. Stein, H. Bockhorn, A. Kronenburg, The role of thermodiffusion and dimensionality in the formation of cellular instabilities in hydrogen flames, Proc. Combust. Inst. 40 (1–4) (2024) 105665.
[15] X. Wen, T. Zirwes, A. Scholtissek, H. Boettler, F. Zhang, H. Bockhorn, C. Hasse, Flame structure analysis and composition space modeling of thermodiffusively unstable premixed hydrogen flames—Part I: Atmospheric pressure, Combust. Flame 238 (2022) 111815.
[16] X. Wen, T. Zirwes, A. Scholtissek, H. Boettler, F. Zhang, H. Bockhorn, C. Hasse, Flame structure analysis and composition space modeling of thermodiffusively unstable premixed hydrogen flames—Part II: Elevated pressure, Combust. Flame 238 (2022) 111808.
[17] C. Matteucci, F. D'Alessio, A. Nicolai, P.E. Lapenna, F. Creta, Marginal stability of thermodiffusively unstable circular expanding flames, Proc. Combust. Inst. 41 (2025) 105920.
[18] F. Zhang, T. Zirwes, Y. Wang, Z. Chen, H. Bockhorn, D. Trimis, D. Stapf, Dynamics of premixed hydrogen/air flames in unsteady flow, Phys. Fluids 34 (8) (2022).
[19] L. Yang, Y. Wang, T. Zirwes, F. Zhang, H. Bockhorn, Z. Chen, Effects of intrinsic instabilities on the response of premixed hydrogen/air conical flames to inlet flow perturbations, Flow, Turbul. Combust. 112 (4) (2024) 1275–1297.
[20] A. Porcarelli, P.E. Lapenna, F. Creta, I. Langella, Stability analysis of thermodiffusively unstable counterflow lean premixed hydrogen flames, Proc. Combust. Inst. 41 (2025) 105906.
[21] G. Sivashinsky, Nonlinear analysis of hydrodynamic instability in laminar flames—I. Derivation of basic equations, Acta Astronaut. 4 (11) (1977) 1177–1206.
[22] G. Sivashinsky, Diffusional-thermal theory of cellular flames, Combust. Sci. Technol. 15 (3–4) (1977) 137–145.
[23] G.I. Sivashinsky, C.K. Law, G. Joulin, On stability of premixed flames in stagnation-point flow, Combust. Sci. Technol. 28 (3–4) (1982) 155–159.
[24] F. Creta, P.E. Lapenna, R. Lamioni, N. Fogla, M. Matalon, Propagation of premixed flames in the presence of Darrieus–Landau and thermal diffusive instabilities, Combust. Flame 216 (2020) 256–270.
[25] P.E. Lapenna, G. Troiani, F. D'Alessio, F. Creta, Modeling aspects of thermodiffusively unstable turbulent premixed flames, Proc. Combust. Inst. 41 (2025) 105963.
[26] M. Ó Conaire, H.J. Curran, J.M. Simmie, W.J. Pitz, C.K. Westbrook, A comprehensive modeling study of hydrogen oxidation, Int. J. Chem. Kinet. 36 (11) (2004) 603–622.
[27] S. Kadowaki, Numerical study on the instability of premixed plane flames in the three-dimensional field, Nt. J. Heat Fluid Flow 17 (6) (1996) 557–566.
[28] L. De Goey, J. ten Thije Boonkkamp, Mass burning rate of premixed stretched flames: Integral analysis versus large-activation-energy asymptotics, J. Engrg. Math. 62 (1) (2008) 67–84.
[29] J.D. Buckmaster, G.S.S. Ludford, Theory of laminar flames, Camb. N. Y. (1982).
[30] T. Poinsot, D. Veynante, Theoretical and Numerical Combustion, RT Edwards, Inc, 2005.